Journal of Nuclear Materials 455 (2014) 402–406

Contents lists available at ScienceDirect

Journal of Nuclear Materials

journal homepage: www.elsevier.com/locate/jnucmat

Improving high temperature creep resistance of reduced activation steels by addition of nitrogen and intermediate heat treatment

W.B. Liu [a], C. Zhang [a,*], Z.X. Xia [b], Z.G. Yang [a]

[a] Key Laboratory of Advanced Materials of Ministry of Education, School of Materials Science and Engineering, Tsinghua University, Beijing 100084, China
[b] Shagang School of Iron and Steel, Soochow University, Suzhou 215021, China

ARTICLE INFO

Article history:
Available online 27 July 2014

ABSTRACT

In the present study, we report an enhanced high-temperature creep resistance in reduced activation ferrite/martensite (RAFM) steels, by introducing nitrogen (0.035 wt%, M3 steel) and employing a novel intermediate heat treatment I–Q–T (intermediate treatment, quenching and tempering). In comparison with all the control groups, the uniaxial tests of the I–Q–T treated M3 steel showed significant increase in rupture time and decrease in elongation. The microstructures of the samples were further characterized to elucidate the origin of the enhanced creep resistance. It is found that, by introducing nitrogen, the primary TaC particles were refined; by employing the I–Q–T heat treatment, the dispersed fine secondary MX precipitates, as well as the lath subgrains containing high-density dislocations, were increased: all are responsible for the improved creep resistance.

1. Introduction

Reduced activation ferrite/martensite (RAFM) steels (Fe–Cr–W–V–Ta) have potential applications as first wall and blanket structure materials in fusion reactors [1]. RAFM steels show excellent high temperature strength because of their complex microstructures consisting of high-density dislocations, sub-boundaries decorated with $M_{23}C_6$ carbides and intragranular regions containing MX-type (Ta, V) carbides/nitrides [2,3]. In the past decades, the creep resistance of ferrite/martensite 9–12 wt% Cr steels have been extensively investigated, including effects of initial microstructures (such as dislocations, grain boundaries and carbides), experimental conditions (such as strain rates and temperatures) and the alloying element types (such as Cr, W, Ta, and B) [4–11]. Because of the long-term exposure to high temperatures (500–600 °C) [4,5], there is a strong demand for further improving the creep resistance of RAFM steels.

It is confirmed that controlling the type and size of precipitates is critical to control the creep resistance of RAFM steels, and dispersed fine MX carbide, such as TaC, is critical to improve the creep resistance [6–8]. However, the addition of Ta to steels causes the formation of coarse primary TaC particles, and the addition of more carbon to a 9% Cr steel triggers the formation of a large amount of $M_{23}C_6$ carbides. Both the primary TaC particles and $M_{23}C_6$ carbides are deleterious to the mechanical properties. Act as a primary forming element of TaX (X = C, N) carbide in steels [12], nitrogen is a promising candidate element that can be selected to avoid the formation of these two precipitates. Although some work has been done to control the TaX precipitates during intermediate heat treatment [13], the effect of nitrogen and intermediate heat treatment on creep resistance was still not clearly illustrated. In the present work, creep resistances and the microstructural development of two different types of RAFM steels (with and without the addition of nitrogen) were studied.

2. Experimental

Two RAFM steels, M2 steel (without nitrogen) and M3 steel (with 0.035 wt.% nitrogen), studied in the present work, were melted in a vacuum induction furnace into an ingot weight 25 kg, followed by hot-forging and rolling into a 15-mm-thick plate. The chemical compositions of the melted steels are shown in Table 1.

The heat treatment processes used in the present work are shown in Fig. 1 [13], which includes (a) austenitization at 980 °C for 45 min followed by air cooling to room temperature (quenching, defined as Q), and then tempering at 760 °C for 90 min (tempering, defined as T); (b) the steels were moved to a furnace preheated to 850 °C for 20 min after the usual austenitization at 980 °C for 45 min (intermediate treatment and quenching, defined as I–Q), followed by tempering at 760 °C for 90 min (tempering, also defined as T). All processes were air cooled to room temperature. The selection of 850 °C as intermediate heat treatment tem-

* Corresponding author. Tel.: +86 (010) 62797603.
E-mail address: chizhang@tsinghua.edu.cn (C. Zhang).

http://dx.doi.org/10.1016/j.jnucmat.2014.07.040
0022-3115/

Table 1
Chemical composition (mass fracture %) of tested steel.

Steel	C	Cr	Mn	Ta	W	V	N	Fe
M2	0.088	8.75	0.49	0.28	1.59	0.21	–	Bal
M3	0.073	8.77	0.48	0.26	1.59	0.21	0.035	Bal

perature was determined according to the calculation results of JMatPro [13].

Heat treated samples were studied with scanning electron microscope (SEM) of type JEOL JSM-7000. The samples for SEM were ground and mechanically polished. The polished samples were etched in a particular solution (12 ml alcohol + 3 ml hydrochloric acid + 1 g ferric trichloride) to observe the microstructure and morphology of matrix and carbides. Microstructures of the samples were also characterized by transmission electron microscopy (TEM) on JEOL Tecnai F20. The TEM samples were obtained by means of cutting, grinding and thinning at low temperatures. Energy dispersive spectroscopy (EDS) in SEM and TEM was also used to identify the different types of carbides with various sizes. The uniaxial creep tests were performed at 550 °C with an applied stress of 270 MPa using the standard specimen machined to 10 mm in diameter and 100 mm in gauge length.

3. Results and discussion

3.1. Result of uniaxial tensile creep tests

Results of uniaxial tensile creep tests conducted at 550 °C under 270 MPa are shown in Fig. 2. As demonstrated in the figure, M3 steels have better creep resistance than M2 steels for both the rupture time and the elongation. For M2 steels, the rupture time increased slightly from 12.8 h for Q–T treatment to 15.1 h for I–Q–T treatment, while the elongation remained almost unchanged for both treatments. For M3 steels, both samples did not rupture even after 27 h, whereas the elongation for I–Q–T treatment was 2.75%, which is significantly lower than 4.80% for Q–T treatment (Fig. 2(b)). Therefore, the creep resistance has been further improved for both steels by using intermediate heat treatment.

3.2. Characterization after Q and I–Q: effect of N content

TEM images after Q and I–Q treatments for all samples are shown in Fig. 3. Typical quenched martensite laths with dispersed fine precipitates were found in all pictures. However, coarse particles, with size ~500 nm in the long axis, were found in M2 steel for both Q and I–Q samples (Fig. 3(a) and (b)). These particles were further identified by EDS as primary TaC particles formed during melting process. In contrast, the precipitates are finer in M3 steels, and there are more fine precipitates inside grains and/or along grain boundaries after I–Q (Fig. 3(d)) than those after Q (Fig. 3(c)).

As is shown in Table 1, M3 steel had additional nitrogen, whereas the remaining elements were the same in both steels. Ta plays an important role in lowering DBTT through its effect on prior-austenitic grain size refinement [5], and the content of Ta is usually in the range from 0.02 to 0.18 wt% in traditional RAFM steels. Coarse TaC particles were found in M2 steel because of the low solubility of Ta in the matrix (Fig. 3(a) and (b)). The TaC particles were regarded as primary MX carbide, which formed during melting stage. However, coarse TaC particles were hardly observed in M3 steels (Fig. 3(c) and (d)).

MX carbonitrides play an important role in improving the creep resistance, and nitrogen is considered as primary forming element of TaX (X = C, N) in RAFM steels [12]. Vanaja et al. [5] pointed out that the RAFM steel with 0.06% tantalum had better creep resistance than that of steel with 0.14% tantalum. They thought that lar-

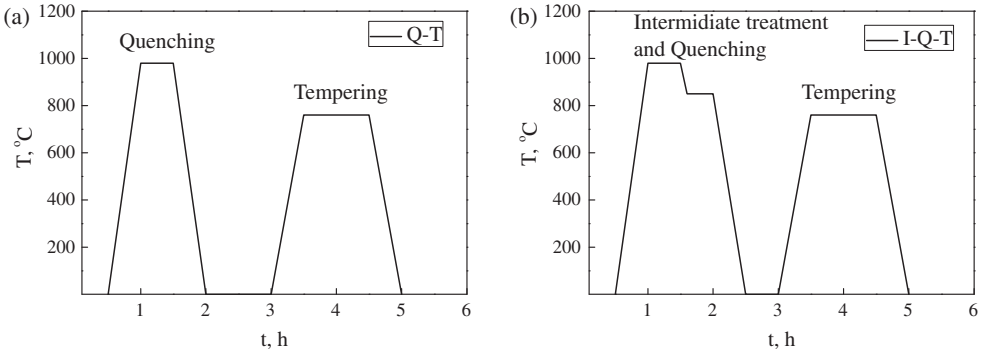

Fig. 1. Schematic diagram of the intermediate heat treatment and tempering treatment (Q = water quenching, I = intermediate treatment, T = tempering). (a) Q–T, (b) I–Q–T.

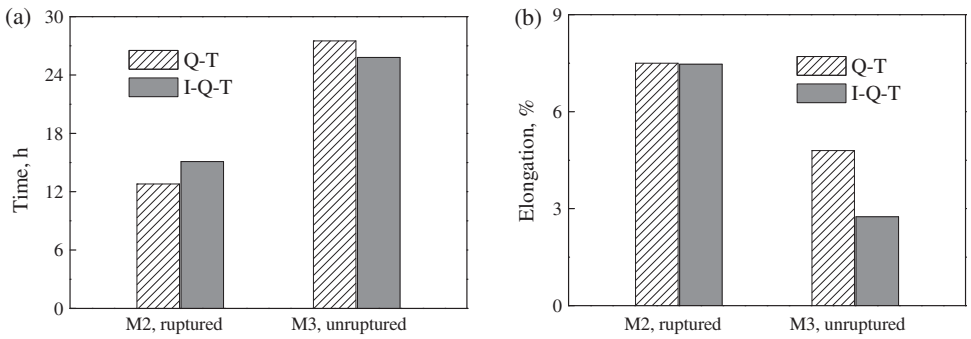

Fig. 2. Results of creep experiments (550 °C, 270 MPa) (a) experiment time and (b) elongation of the samples.

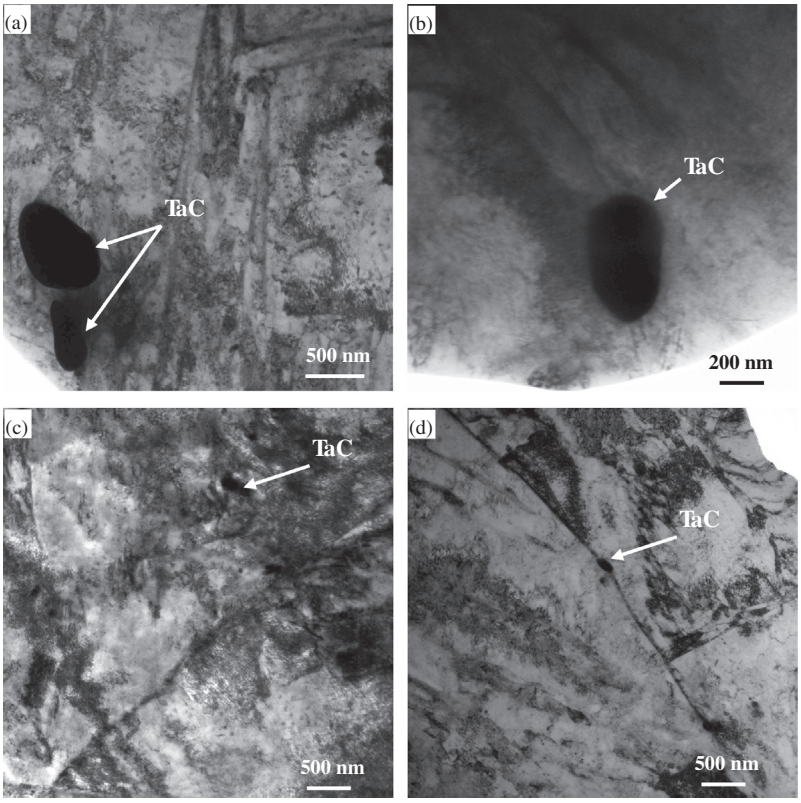

Fig. 3. TEM images after Q (a), (c) and I–Q (b), (d) treatment for M2 steel (a), (b) and M3 steel (c), (d).

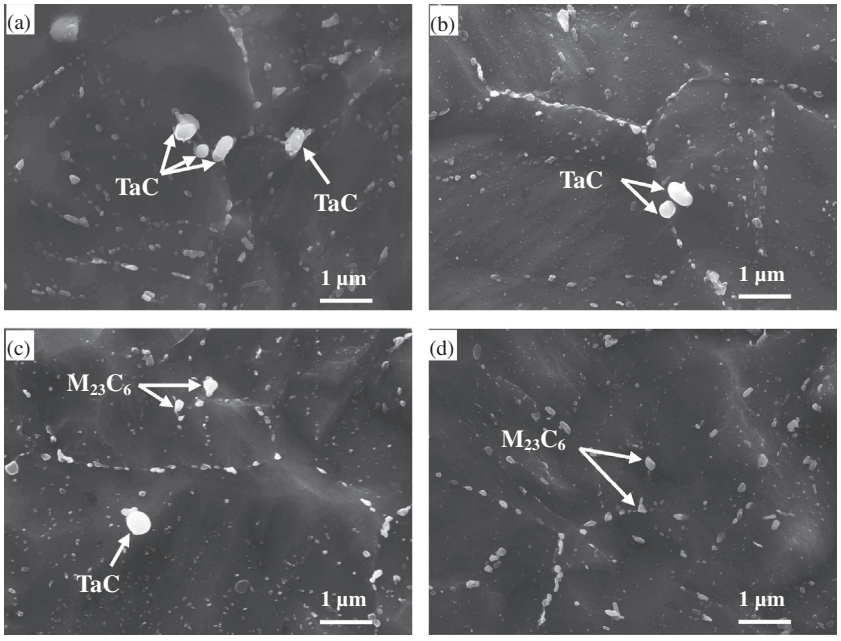

Fig. 4. SEM images after Q–T (a), (c) and I–Q–T (b), (d) treatment for M2 steel (a), (b) and M3 steel (c), (d).

ger amount of carbon would be locked as primary TaC in steel having higher tantalum content, and hence the higher tantalum content in RAFM steel reduces the creep rupture strength. Additional nitrogen in M3 steel increases the solubility of Ta in the matrix. Therefore, no coarse primary TaC particles were observed from the SEM and TEM figure of M3 steels, and more dispersed MX carbonitrides were found, which give the M3 steels better creep resistance.

3.3. Characterization after Q–T and I–Q–T: effect of intermediate treatment

SEM images after Q–T and I–Q–T treatment for all the samples are shown in Fig. 4. Precipitates of different sizes, which mainly formed during temper treatment, are seen in the figures. Larger particles distributed along the lath, block, packet boundaries and the prior austenite grain boundaries (PAGBs) were determined as

the $M_{23}C_6$ carbides by EDS, while the finer precipitates in the grains were mostly MX carbonitride. Coarse TaC particles as large as 500 nm in the long axis were still observable after tempering (Fig. 4(a) and (b)), and it was confirmed that the coarse TaC particles formed during melting cannot be refined during subsequent tempering because of the slow diffusivity of Ta. As mentioned and discussed earlier, after quenching or intermediate treatment, the TaC particles in M3 steels (Fig. 3(c) and (d)) are much smaller than that in M2 steels (Fig. 3(a) and (b)). Therefore, primary coarse TaC particles can be hardly found in M3 steels after tempering (Fig. 4(c) and (d)), either. It should be mentioned that the mean size of $M_{23}C_6$ after I–Q–T (Fig. 4(d)) is smaller than that after Q–T (Fig. 4(c)), since larger amount of carbon and nitrogen would be locked as secondary TaC during intermediate treatment at 850 °C.

TEM images of steel microstructure and carbides after I–Q–T for the two steels are shown in Fig. 5. Small precipitates distributed along the lath, block and packet boundaries were observed (Fig. 5(a) and (c)) after I–Q–T. Compared with the small dispersed precipitates (~20 nm) in M3, carbides with size between 100 and 200 nm were observed in M2 steel. The carbides were further determined as Ta-riched particles and W-riched particles by EDS (Fig. 5(b)).

Dispersed fine precipitates were critical to improve the creep resistance. $M_{23}C_6$ carbides along lath and block boundaries can produce sub-boundary hardening and precipitation hardening in creep-resistant steels. Abe et al. [6–8] pointed out that the suppression of particle coarsening during creep and the maintenance of a homogeneous distribution of $M_{23}C_6$ carbides near prior austenite grain boundaries are effective for preventing the long-term degradation of creep strength and for improving long-term creep strength. In 9–12% Cr steels, however, the coarsening rate of $M_{23}C_6$ carbides is much larger than that of MX type precipitates [1,14]. Therefore, the long-term stabilization of fine precipitates, such as TaC, is a key issue for suppressing the loss of creep strength [14]. As mentioned earlier, more dispersed fine MX carbonitrides formed when applying the intermediate heat treatment, and thus creep resistances were improved for both of the steels by I–Q–T.

3.4. Dislocations and carbides

TEM images of the dislocations and STEM images of carbides in M3 steel after I–Q–T are shown in Fig. 6. High density of dislocations were observed in M3 steel (Fig. 6(a)), and the finer precipitates were determined as $M_{23}C_6$ and TaC by STEM and EDS (Fig. 6(b)).

Both Cr rich $M_{23}C_6$ carbides and Ta rich MX carbonitrides can form during tempering in martensitic 9–12% Cr steels. The favorable nucleation sites of precipitates, determined by the free energy, in sequence were inclusion boundaries, grain boundaries (GBs), twin boundaries, dislocations, vacancies, and matrix [15]. Because of the high interfacial free energy of the GBs, the precipitates stabilize and coarsen on the grain boundaries after a diffusion-controlled ripening. Moreover, the diffusivity of Cr atoms along the PABGs is faster than that in the matrix. Therefore, the size of $M_{23}C_6$ carbides distributed along PAGBs is usually much larger than that inside grains after tempering. Nevertheless, the size of carbonitrides is much smaller than that of $M_{23}C_6$ carbides because of the much lower coarsening rate of carbonitrides. Most of the $M_{23}C_6$ carbides are distributed along laths, blocks, packet boundaries and PAGBs, while the MX carbonitrides are distributed within the matrix.

It is reported that the coarsening rate of $M_{23}C_6$ carbides is much higher in the vicinity of PAGBs than within grains [8], because diffusion along the PAGBs is faster. In 9–12% Cr steels, the coarsening

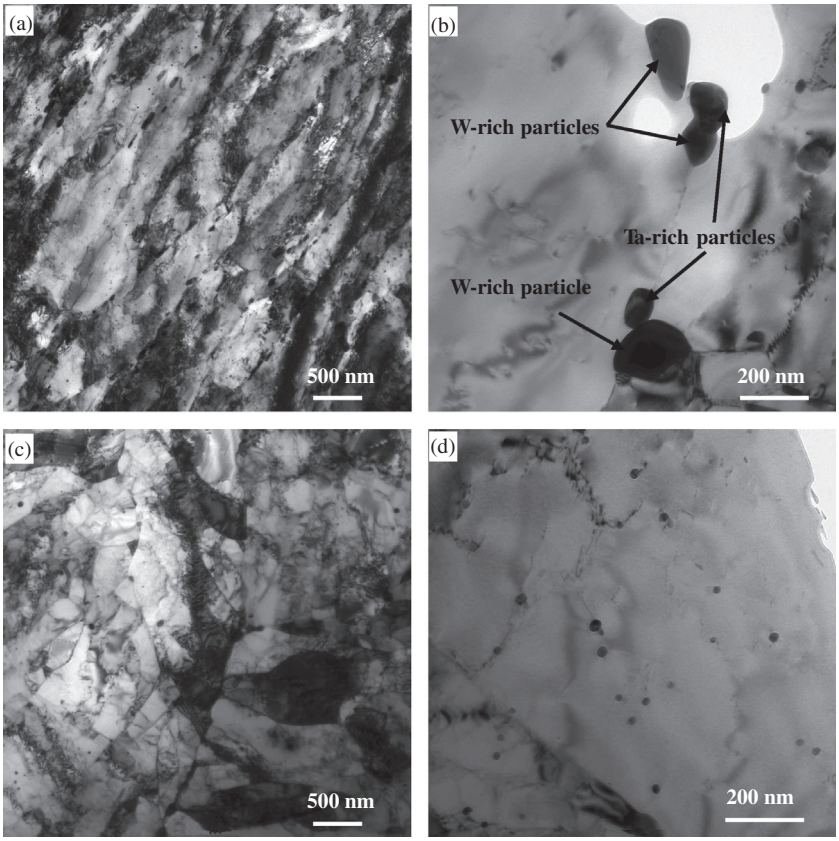

Fig. 5. TEM images of microstructures (a), (c) and carbides (b), (d) after I–Q–T for M2 steel (a), (b) and M3 steel (c), (d).

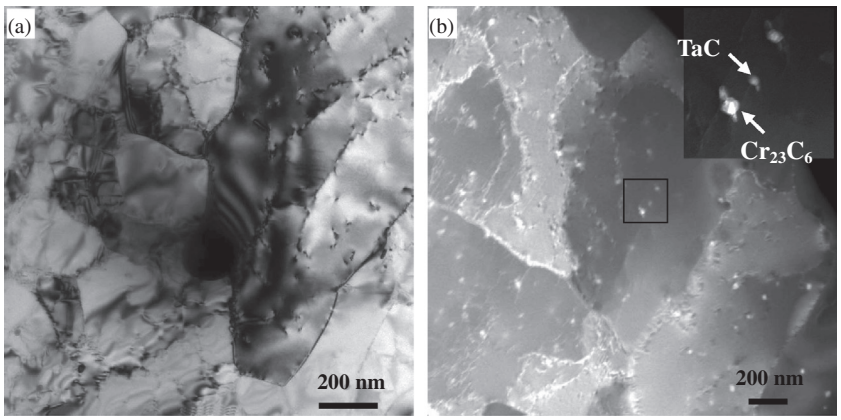

Fig. 6. TEM images of dislocations (a) and STEM images of carbides (b) after I–Q–T for M3 steel, inset in (b) shows a locally magnified picture.

rate of MX type precipitates can be as low as 1/10 of that of $M_{23}C_6$ carbides [1,14]. Therefore, the long-term stabilization of fine precipitates, particularly those near PAGBs, is a key issue for suppressing the loss of creep strength [7,14]. Results from Vanaja et al. [5] showed that the fine secondary VC carbides, which precipitate during tempering, play a more important role in imparting the creep strength than the TaC precipitates, since they exhibit a very low coarsening rate during exposure at elevated temperatures. However, the addition of carbon to a 9% Cr steel causes the formation of a large amount of $M_{23}C_6$ carbides. Abe et al. [6–8] suggested that one can almost exclusively obtain vanadium nitrides after tempering by reducing the carbon concentration to very low amounts below 0.02%. This is because the amount of $M_{23}C_6$ carbides decreases with decreasing carbon concentration, while the amount of MX carbonitrides is approximately constant over a wide range of carbon concentration from 0% to 0.15%.

In the present work, the addition of nitrogen (M3 steel) also increased the amount of MX carbonitrides with fine size about 5–20 nm (Fig. 5(d)). The size of $M_{23}C_6$ carbides distributed along PAGBs in nitrogen addition steel also becomes much smaller by I–Q–T treatment (Fig. 4(d)), because most of the carbon and nitrogen atoms in the steels precipitate as carbides and nitrides during intermediate treatment at 850 °C.

Dislocation hardening is useful for creep strengthening, and tempered martensitic 9–12% Cr steels usually contain a high density of dislocations in the matrix even after tempering, usually in the range of $1–10 \times 10^{14}$ m^{-2} [6]. Lath subgrains, which contain a high density of dislocations and fine precipitates are found in the present M3 steel after I–Q–T (Fig. 6(a)), which also explain the better creep resistance of the M3 steel.

4. Conclusions

The creep resistance of the RAFM steels was improved with the addition of nitrogen and the application of intermediate heat treatment. Because of the addition of nitrogen, primary TaC in M3 steel (nitrogen added) is much smaller than that in M2 steel (without nitrogen). M3 steel showed better creep resistance than the M2 steel for both the rupture time and elongation. After the application of intermediate heat treatment, more dispersed fine secondary MX precipitates and dislocations with high density were found in both M2 and M3 steel, which were critical to improve the creep resistance.

Acknowledgements

Financial support from the National Basic Research Program of China (No. 2011GB108006) and National Natural Science Foundation of China (No. 51071090) is acknowledged. The authors are grateful to Mr. Y.Z. Ji and Mr. S. Salam for their useful discussion and suggestions.

References

[1] W. Yan, W. Wang, Y.Y. Shan, K. Yang, Front. Mater. Sci. 7 (2013) 1–27.
[2] F. Abe, T. Noda, H. Araki, S. Nakazawa, J. Nucl. Mater. 179–181 (1991) 663–666.
[3] F. Abe, T. Noda, M. Okada, J. Nucl. Mater. 195 (1992) 51–67.
[4] R.L. Klueh, D.J. Alexander, M.A. Sokolov, J. Nucl. Mater. 304 (2002) 139–152.
[5] J. Vanaja, K. Laha, M.D. Mathew, T. Jayakumar, E.R. Kumar, Proced. Eng. 55 (2013) 271–276.
[6] F. Abe, Sci. Technol. Adv. Mater. 9 (2008) 013002.
[7] F. Abe, Mater. Sci. Eng., A 510–511 (2009) 64–69.
[8] F. Abe, M. Taneike, K. Sawada, Int. J. Pres. Ves. Pip. 84 (2007) 3–12.
[9] J. Pesicka, R. Kuzel, A. Dronhofer, G. Eggeler, Acta Mater. 51 (2003) 4847–4862.
[10] J. Vanaja, K. Laha, S. Sam, M. Nandagopal, S.P. Selvi, M.D. Mathew, T. Jayakumar, E.R. Kumar, J. Nucl. Mater. 424 (2012) 116–122.
[11] J. Vanaja, K. Laha, M. Nandagopal, S. Sam, M.D. Mathew, T. Jayakumar, E.R. Kumar, J. Nucl. Mater. 433 (2013) 412–418.
[12] P. Hua, W. Yan, L.F. Deng, W. Sha, Y.Y. Shan, K. Yang, Fusion Eng. Des. 85 (2010) 1632–1637.
[13] Z.X. Xia, C. Zhang, N.Q. Fan, Y.F. Zhao, F. Xue, S.J. Liu, Mater. Sci. Eng., A 545 (2012) 91–96.
[14] M. Taneike, F. Abe, K. Sawada, Nature 424 (2003) 294–296.
[15] K. Mo, G. Lovicu, H.M. Tung, X.A. Chen, J.F. Stubbins, J. Eng. Gas. Turb. Power 133 (2011) 052908.